Research Article | Vol. 9, No. 5 / 1 May 2019 / Optical Materials Express 2252
Optical Materials EXPRESS

Understanding aging in chalcogenide glass thin films using precision resonant cavity refractometry

Sarah Geiger,[1,2,5] Qingyang Du,[2] Bin Huang,[2] Mikhail Y. Shalaginov,[2] Jérôme Michon,[2] Hongtao Lin,[3] Tian Gu,[2] Anupama Yadav,[4] Kathleen A. Richardson,[4] Xinqiao Jia,[1] and Juejun Hu[2,6]

[1]*Materials Science and Engineering Department, University of Delaware, 201 DuPont Hall, Newark, DE 19716, USA*
[2]*Department of Materials Science and Engineering, Massachusetts Institute of Technology, 77 Massachusetts Avenue, Cambridge, MA 02139, USA*
[3]*College of Information Science & Electronic Engineering, Zhejiang University, Hangzhou, China*
[4]*CREOL, The College of Optics and Photonics, University of Central Florida, 4304 Scorpius Street, Orlando, FL 32816-2700, USA*
[5]*sjgeiger@udel.edu*
[6]*hujuejun@mit.edu*

Abstract: Chalcogenide glass (ChG) thin films have a wide range of applications in planar photonics that rely on the stability of their optical properties. However, most methods do not provide quantitative optical property data at sufficiently high resolution. We have employed a resonant cavity refractometry technique capable of detecting refractive index changes down to 10^{-6} refractive index unit (RIU) to study the aging, or sub-T_g structural relaxation kinetics, of $Ge_{23}Sb_7S_{70}$ ChG. Our study reveals that the refractive index (RI) change due to aging tends to follow stretched exponential behavior, with stretch exponents and rate of index change dependent on initial glass treatment. Thermally annealed devices show the best stability, suggesting that thermal annealing is the appropriate post-deposition treatment method for obtaining stable ChG films.

1. Introduction

Glasses are inherently thermodynamically metastable. The thermodynamic instability and excess free enthalpy of glasses below their glass transition temperature (T_g) leads to physical aging effects over time as the glass structure relaxes towards a more thermodynamically stable state [1–4]. Concurrent with glass aging are changes to the structural, mechanical, thermal and optical properties of glasses, and thus understanding the aging process is essential to both fundamental glass science and practical applications involving glass materials. The earliest observation of glass aging was measured by Joule, who tracked the zero-point displacement of a thermometer over time [5]. Today, physical aging of glasses is traditionally measured by tracking changes in enthalpy loss or fictive temperature of the glass using differential scanning calorimetry (DSC), with experiments often spanning decades. These experiments have shown that enthalpy relaxation proceeds by a stretch exponential (Kohlrausch) function defined by a Kohlrausch exponent, β, with the form:

$$e^{-(t/\tau)^{\beta}} \tag{1}$$

Values of β for glass materials tend to fall on or near select 'magic numbers' that correspond with the axiomatic Phillips fields-free diffusion-to-traps model of structural relaxation, initially derived from charge diffusion experiments [6,7]. These magic numbers are predicted theoretically by

#360608 https://doi.org/10.1364/OME.9.002252
Journal © 2019 Received 20 Feb 2019; revised 29 Mar 2019; accepted 2 Apr 2019; published 17 Apr 2019

Optical Materials EXPRESS

assuming that the structural relaxation mechanism is dependent on the effective dimensionality (d) of the configuration space in which the diffusion occurs:

$$\beta = \frac{d}{d+2} \tag{2}$$

Of particular interest for network glasses are $\beta = 3/5$ and $\beta = 3/7$. $\beta = 3/5$ corresponds to a system where d = 3, undergoing structural relaxation dominated by short-range forces, while $\beta = 3/7$ corresponds to d = 3/2, signals a system dominated by a mixture of short and long-range forces. In chalcogenide glass short range forces are said to indicate relaxation between covalent bonds, while a mixture of short- and long-range forces indicate interchain relaxation of the glass [6,8,9].

In this study, we focus our attention on aging of chalcogenide glasses (ChGs), the amorphous compounds containing the chalcogen elements S, Se, and/or Te. The ChGs are a group of glass materials of significant interest to both glass science and optical applications. For instance, ChGs are known for their large capacity for compositional alloying. This unique attribute allows continuous modification of their network structures and thus presents them as an ideal system for investigating the impact of network topology on physical aging [10]. Constraint within the glass matrix is typically quantified by the number of Lagrangian constraints per atom (n_c), with the ideally constrained ChG matrix having $n_c = 3$. This is related to the average coordination number, Z, bonds per atom, with a critically constrained ChG matrix having Z = 2.4. Above Z = 2.4, the glass network is over-constrained and aging effects are less energetically favorable. Below Z = 2.4, aging can proceed at ambient conditions at expedited rates, making these glass materials unsuitable for applications where material stability is necessary [11–13].

In addition, the relatively weak chemical bonding between chalcogens and other atoms as compared to those in oxide glasses implies that aging of ChG is strongly dependent on the processing history and storage conditions of the glass. For instance, exposure to light near the bandgap of the glass causes photobleaching (or photodarkening) and light-assisted aging [14]. Annealing below the glass transition temperature (T_g) allows them to settle to a more thermodynamically favorable state [13–16]. Exposure to air leads to water absorption or oxide formation on the surface of the glass [17–20]. Therefore, understanding the interplay between glass processing and aging kinetics is an important topic for ChGs.

From the perspective of practical applications, studying the aging kinetics of ChGs is also highly relevant to many optics and photonics applications. Key to predicting the optical performance in molded bulk optics is the need to quantify the refractive index change (usually a decrease) associated with the thermal history 'reset' or 'rejuvenation' imparted through the precision glass molding (PGM) protocols used to reheat and shape the optical element. A variety of studies have looked at such relaxation processes and the understanding assists in predictably understanding optical property stability in these bulk applications [12–15,21,22]. With their large infrared transparency windows, high nonlinearity, and compatibility with standard microfabrication techniques, ChGs have a wide range of state-of-the-art applications in optics and photonics. They can be easily processed into a wide range of photonic devices such as waveguides [23–32], Bragg gratings [33,34], resonators [35–39], micro-lenses [40–44], omnidirectional reflectors [45–47], and photonic crystals [48–51]. Their nonlinear characteristics also make them promising candidates for all-optical signal processing [52,53] and nonlinear frequency generation [54–57]. Further, their photosensitivity may be leveraged in the device patterning using laser direct writing [58–60]. Taking advantage of their low deposition temperatures, it has been further demonstrated that ChG devices can be patterned on unconventional substrates such as polymers and 2-D materials, which have applications in packaging, conformal epidermal sensing, high-speed data communications, and more [61–67]. Most of these applications mandate long-term stability of the optical properties of ChGs to varying degrees: for example, Bragg gratings, resonator sensors, and photonic crystal switches are particularly sensitive even to minute changes in refractive indices. Aging is known to change the refractive index of the glass [68,69], resulting in

Optical Materials EXPRESS

deleterious wavelength drift and performance degradation in photonic devices over time. This effect is sometimes even cited as a main drawback against the utility of chalcogenide glasses in optics and photonics, given their reduced T_g and expedited aging compared to their oxide counterparts [70].

Despite the recognized importance of understanding and quantifying the aging process in ChGs (as well as other optical glasses), few experiments have directly tracked the optical property evolution of glasses over time. A main technical challenge lies in the small magnitude of the changes. Changes of the real part of the refractive indices due to aging are usually in the order of 10^{-3} to 10^{-4} (refractive index unit or RIU), comparable to the resolution of classical thin film optical measurement techniques such as ellipsometry or prism coupling. Moreover, the relaxation of some glasses can take decades to stabilize. The result of this is the limited set of optical aging measurements reported in literature. Many involve scattered optical measurements spaced out over years in order to observe any significant changes with these techniques [12,15,71,72]. The limited resolution also excludes precise quantification of the aging kinetics. Furthermore, the reported measurements were performed on films exposed to environmental conditions that do not mirror the storage and geometry of real ChG devices.

One commonly adopted procedure enabling the study of slow material (or device) aging or degrading processes within an acceptable timeframe is accelerated aging test, where the kinetics of the process is expedited by exposing the subject material to elevated temperatures. Glass aging follows non-Arrhenius behavior below T_g, and thus at different temperatures different thermodynamically stable states of the glass are accessed and the selection of an appropriate aging temperature is not straightforward [73–78]. In actual photonic devices where ChGs are inevitably used alongside other materials, the situation is further complicated as heat treatment can result in significant thermal stress which further modifies the equilibrium states the glass relax towards at different temperatures [79].

Here we quantified the aging kinetics of ChG thin films and its dependence on processing conditions using resonant cavity refractometry [35,80]. In resonant cavity refractometry, the changes in the optical characteristics of a cavity are tracked via its resonant wavelength shift. Previous resonant cavity refractometry techniques track the optical changes of a single cavity over time, in most cases describing only the stability of the resonator as a whole and not capturing the changes in the cavity material itself [33,81]. Prior work on resonant cavity refractometry investigated photosensitivity in ChG-based resonators, which indicates a photosensitive refractive index change in the order of 10^{-2}. The approach used, however, is not adequately precise for aging studies as aging of cladding materials can also contribute to resonance drift and interfere with the refractive index change quantification [35].

In this technique, tiny refractive index changes in a ChG are monitored through tracking the resonant wavelength shifts of optical cavity arrays of four ChG devices. Each array undergoes different processing conditions before aging is tracked. Since the resonant wavelength of an optical cavity with high quality factor (Q-factor) can be determined with picometer-level accuracy, the technique features exceptional resolution to refractive index changes (down to 10^{-5} RIU and below [35,80]) ideal for probing the kinetics of aging processes. Furthermore, the technique also measures aging of ChG when the material is deployed in a functional photonic device and therefore the results are immediately relevant to device applications based on ChGs.

2. Experimental details

In this study, we chose $Ge_{23}Sb_7S_{70}$ (GSS, bulk composition) as our model system since it has been shown to be non-toxic [82], resistant to oxidation, and applicable to fabricating champion low-loss devices with a diverse range of applications [83,84]. Its average coordination number is $Z = 2.53$, thus the network should be somewhat overconstrained and age slowly. It has a T_g of 311°C [85], much higher than common As-based ChGs (the T_g's of As_2S_3 and $As_{40}Se_{60}$

Optical Materials EXPRESS

are 210°C and 187°C [18,86], respectively), which implies reduced aging at room temperature essential for practical device applications. The refractive index of thermally evaporated GSS is approximately 2.22 at 1550 nm, and the expected composition post-evaporation is $Ge_{23}Sb_{11}S_{66}$ [87]. Figure 1(A) schematically illustrates the layout of the micro-ring cavity device used for refractometry measurements.

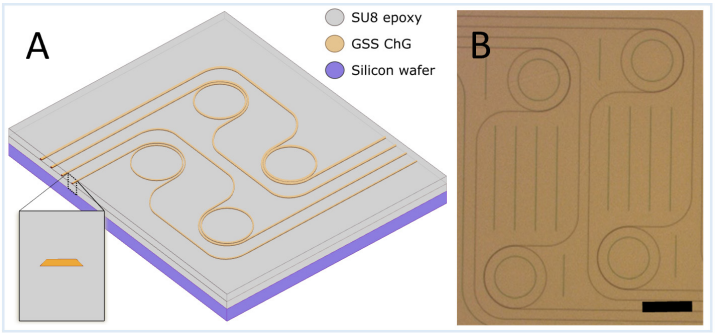

Fig. 1. A) 3D perspective drawing of the device arrays used in this experiment. B) Optical microscope image of the device chip (Scale bar 300 µm).

The waveguides and micro-ring resonators were fabricated using electron beam lithography and a lift-off technique [88]. We select lift-off over etching because lift-off yields a pristine glass surface without excess materials (e.g. fluorine sidewall coatings [89]) that can complicate the analysis. First, a silicon wafer coated with 150 nm oxide was cleaned in Nanostrip 2X at 80 °C for 5 minutes and rinsed thoroughly in DI water. The wafer was then treated for 30 s with oxygen plasma to improve SU-8 adhesion. 2 µm of SU-8 was spin cast onto the wafer as the bottom cladding layer and soft-baked for 1 minute at 95 °C. This layer was then exposed to 100 mW/cm^2 UV using a Neutronix-Quintel NXQ8006 mask aligner and baked for an additional 150 s at 95 °C. Additional lines were patterned in the regions between devices to aid liftoff, as seen in Fig. 1(B). Next, 500 nm of LOR 5A liftoff resist was spin cast on top of the SU-8 under-cladding and baked for 5 minutes at 150 °C. This was followed by 280 nm of CSAR ARP-6200.09, baked for another 5 minutes at 150 °C. Following electron beam patterning with a Vistec EBPG5200ES, the CSAR resist was developed for 60 s in AR-600-546 developer. The exposed LOR was developed for approximately 35 s to realize a good undercut profile. 250 nm thick GSS was deposited onto the device pattern via thermal evaporation, and the remaining resist and excess glass were lifted off in NMP at 75 °C for approximately 2 minutes. Another 2 µm layer of SU-8 was spun and crosslinked as a top cladding layer using the methods described previously.

We specifically design the waveguide to be symmetrically cladded with SU-8 epoxy to serve two purposes. We have experimentally proven that SU-8 acts as an excellent barrier to moisture in the ambient environment, thereby preventing humidity change from interfering with the measurement. More importantly, as the symmetric waveguide only consists of two materials, ChG and SU-8, we can readily isolate the index change induced by the ChG core. Confinement factors in the ChG core (Γ_{ChG}) and SU-8 cladding (Γ_{SU8}) change with varying waveguide widths and the corresponding resonant wavelength shift ($\Delta\lambda_r$) is given by:

$$\Delta\lambda_r = \frac{\Gamma_{ChG} \times \Delta n_{ChG} + \Gamma_{SU8} \times \Delta n_{SU8}}{n_g} \times \lambda_r \tag{3}$$

Where n is the index of the waveguide core (ChG) or cladding (SU8) and n_g is the group index, given by:

$$n_g = \frac{{\lambda_r}^2}{FSR \times L} \tag{4}$$

Optical Materials EXPRESS

where FSR, or Free Spectral Range, of the resonator corresponds to resonant peak spacing in the wavelength domain, and L is the length of the resonant cavity.

Here we take advantage of the linear relationship between the confinement factor and effective index change of the waveguide mode in order to extrapolate the index change of the glass itself. The core and cladding confinement factors for TE and TM modes in each waveguide geometry were determined by FDTD simulations, shown in Fig. 2. The waveguide profiles analyzed are extracted from SEM images of true device cross-sections. Sidewall angles were approximately 65°.

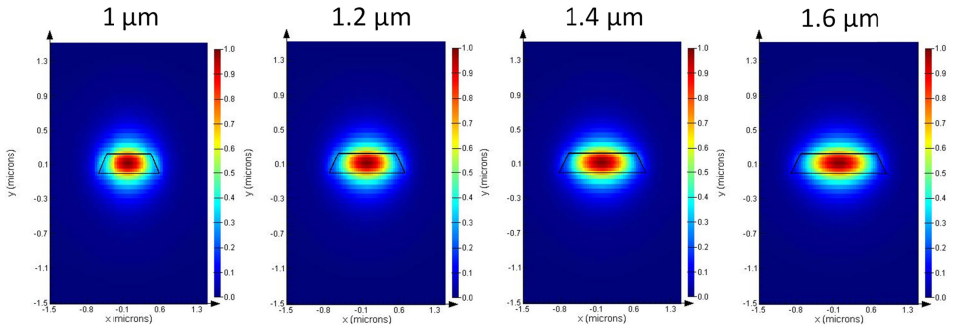

Fig. 2. TE mode profiles for each waveguide simulated with FDTD. The labeled widths are the approximate width of each waveguide at $1/2$ its thickness.

Here we define the normalized confinement factor in the ChG core as:

$$\Gamma_{norm} = \frac{\Gamma_{ChG}}{\Gamma_{ChG} + \Gamma_{SU8}} \tag{5}$$

These values are shown in Fig. 3. Small differences in the waveguide profile geometry due to variations in the liftoff resist profile led to the error shown in the average confinement factor.

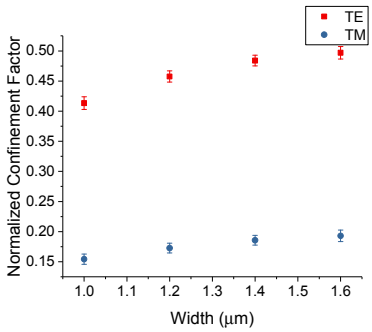

Fig. 3. Average calculated normalized confinement factor for each waveguide width and polarization

We note that $\Gamma_{ChG} + \Gamma_{SU8}$ is a function of waveguide width and in general does not equal to unity due to the slow light effect [90]. Eq. 3 then can be re-written as:

$$\frac{n_g}{\lambda_r} \cdot \frac{\Delta\lambda_r}{\Gamma_{ChG} + \Gamma_{SU8}} = \Gamma_{norm} \times \Delta n_{ChG} + (1 - \Gamma_{norm}) \times \Delta n_{SU8} = (\Delta n_{ChG} - \Delta n_{SU8}) \times \Gamma_{norm} + \Delta n_{SU8} \tag{6}$$

The equation indicates that for each waveguide width, $\frac{\Delta\lambda_r}{\Gamma_{ChG}+\Gamma_{SU8}}$ linearly scales with Γ_{norm} of the waveguide. By plotting $\frac{\Delta\lambda_r}{\Gamma_{ChG}+\Gamma_{SU8}}$ versus the normalized confinement factor, we can therefore extrapolate the refractive index change of the ChG core at $\Gamma_{\mathrm{norm}} = 1$.

Optical Materials EXPRESS

In this study, we track the aging of three groups of devices, each patterned on one chip with identical fabrication protocols but treated with unique initial conditions. The devices were covered with thick opaque tape (Scotch 'Super 33+' Vinyl Electrical Tape) throughout the aging measurements in order to isolate the observed aging effects from photobleaching of the GSS glass [91]. One group of devices was photo-saturated under a broadband halogen lamp used for microscope illumination for 96 hours with a power flux of 4.45 mW/cm^2, determined at 635 nm with a thermal power meter, before covering the device chip with tape and starting aging measurements. The refractive index change of ChG in this group was also tracked during photo-saturation. The next group was covered and measured immediately after cladding, receiving no additional treatment before beginning the study. The final device group was covered immediately and annealed for two hours at 130 °C before beginning aging measurements.

In order to isolate the aging-induced index change from thermal effects, temperature dependent wavelength shifts (TDWS) of ChG resonators with different waveguide widths were determined on a separate set of calibration devices with identical configurations. The device chip was placed on a temperature-controlled stage, and the peak shift was measured at multiple temperatures between 18 °C and 25 °C. The device was left to stabilize for one hour at each temperature before measurement. We also made sure that index drift resulting from aging during the entire experiment was much smaller than the measured thermo-optic index change. As an example, the temperature-dependent resonant wavelength shifts (TDWS) of each measured calibration device are plotted in Fig. 4. The average TDWS was -0.072 ± 0.005 nm/°C for the TE device modes and -0.150 ± 0.009 nm/°C for the TM device modes. The data point to thermo-optic coefficients of $(6.16 \pm 0.59) \times 10^{-5}$ /°C for GSS and $-(2.13 \pm 0.14) \times 10^{-4}$ /°C for SU-8, on the same order of magnitude as prior reports [37,83,92].

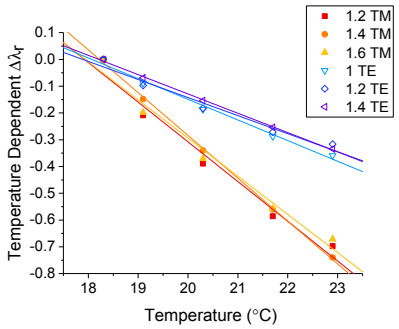

Fig. 4. TDWS of each calibration device with respect to room temperature (18.3 °C)

During aging measurements, the temperature of the stage at each measurement is recorded. In our data analysis, we compensate for the temperature response of each device using the measured TDWS of the calibration device with the same geometry.

3. Results and discussion

During photo-saturation, TE and TM mode confinement factors from four devices with varying widths were analyzed per measurement, calculated from resonant peaks near 1570 nm. The changes in the devices' effective indices versus confinement factors is plotted in Fig. 5(A). The calculated Δn_{ChG} versus exposure dose, extrapolated from the intersection of each best fit line with the $\Gamma_{\mathrm{norm}} = 1.0$ axis, is plotted in Fig. 5(B). The error bars in Fig. 5(B) and Figs. 6 through 8 indicate the standard deviation of the calculated $\Gamma_{\mathrm{norm}} = 1.0$ intercept with the $\frac{n_g}{\lambda_r} \cdot \frac{\Delta\lambda_r}{\Gamma_{ChG}+\Gamma_{SU8}}$ axis. During photo-saturation, the effective index of the GSS decreased and was well fit with a stretch exponential function with a β of 0.495 ± 0.017. The rate constant of this relaxation was a dose

Optical Materials EXPRESS

of 560 ± 51.1 J/cm^2, which corresponded to approximately 36 hours of photo-saturation. This stretch exponent is also in keeping with a similar study done by Knotek *et al.* on $Ge_{24.9}Sb_{11.6}S_{63.5}$ in which the $\beta = 0.45$ for films exposed to several different light intensities at 532 nm [93]. The limit of this fit equation as dose approaches infinity was -(4.596 +/- 0.137) $\times 10^{-2}$ RIU.

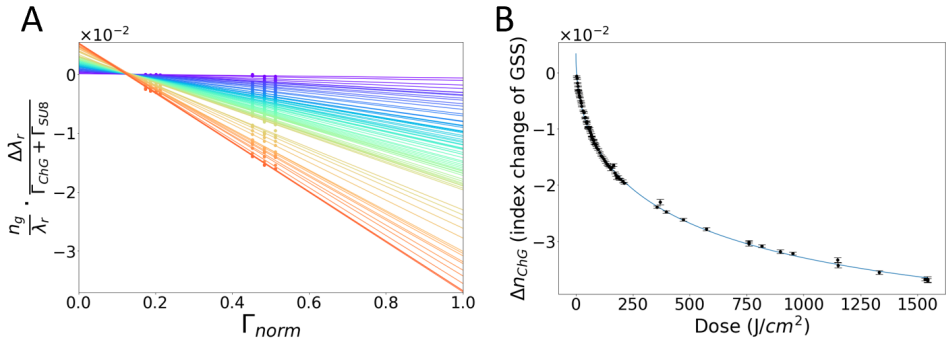

Fig. 5. A) Change in left-hand-side of Eq. 6 versus normalized confinement factor (defined by Eq. 5) during photo-saturation. Data in purple is fit from the earliest time point and red corresponds to the last measurement taken. B) The change in GSS refractive index vs exposure dose of broadband light.

During the aging study of the photo-saturated device, the effective index increased instead of decreased, and changed at a much lower rate than during photo-saturation. Aging of this device was tracked for 32 days. The results, shown in Fig. 6, were best fit by a stretch exponential with $\beta = 0.685 \pm 0.064$ and $\tau_c = 12.4 \pm 2.2$ days. The maximal value of index change as determined by the limit of the stretch exponential fit was (1.335 +/- 0.095) $\times 10^{-3}$ RIU.

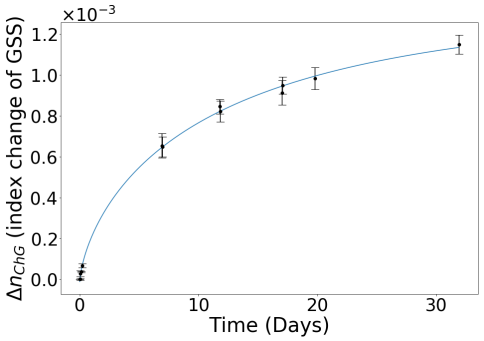

Fig. 6. Refractive index change of GSS as a function of time during aging of photo-saturated devices

The sample that underwent no annealing or photo-saturation prior to beginning the aging study showed the most rapid decrease in Δn_{ChG} during aging. This data, shown in Fig. 7, was fit best by a stretch exponential function with $\tau_c = 32.5 \pm 3.0$ days and $\beta = 0.653 \pm 0.027$. The limit of the refractive index change for this sample was calculated to be -(8.428 +/-0.248) $\times 10^{-3}$ RIU.

In Fig. 8, we observe that the annealed sample showed the smallest change in Δn_{ChG} vs time of all three samples. Over the 18-day time course of this experiment, the data was best fit by an exponential fit instead of a stretch exponential, with $\tau_c = 1.42 \pm 0.25$ days. The limit of index change for this sample was -(1.731 +/- 0.094) $\times 10^{-4}$ RIU.

Overall, aging behavior of both devices that did not undergo heat treatment had stretch coefficients between 0.65 and 0.7, closest to the stretch exponent of 0.6 which indicates structural

Optical Materials EXPRESS

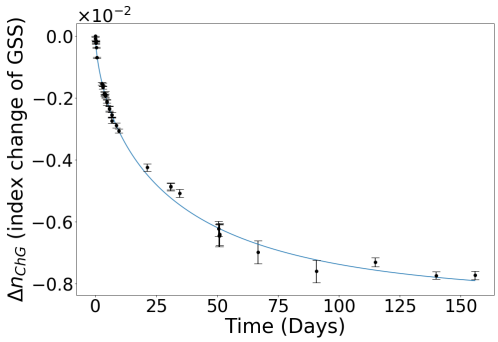

Fig. 7. Refractive index change of GSS as a function of time during aging of untreated devices

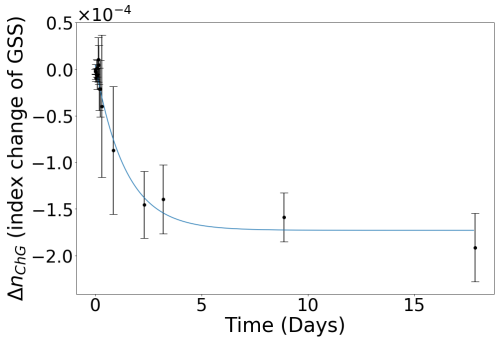

Fig. 8. Refractive index change of GSS as a function of time during aging of annealed devices

relaxation driven by short range forces. This is consistent with a previous report by Knotek *et al.*, who studied aging-induced shifts in the optical bandgap of a $Ge_{24.9}Sb_{11.6}S_{63.5}$ based glass with similar composition [17].

During photo-saturation, the stretch coefficient was closer to $\beta = 0.43$, which would indicate a mixture of short and long-range forces driving index change. The result also suggests that light illumination can produce a structural state significantly different from that in thermally treated but unexposed glasses. Photobleaching, the typical result of exposing many Ge-based ChGs to near-bandgap light, occurred as indicated by the decrease in refractive index. However, the increase in refractive index during aging of this device is somewhat unexpected. The origin of the index increase will be a subject for future studies.

The results from the annealed film are not fit well by a stretch exponential function. This is possibly because the magnitude of the error relative to the glass index change is quite large, with error in many measurements comparable to the index shift. Overall this device had the minimum predicted index change, approximately an order of magnitude less than that of the photosaturated device.

These studies were all continued past the time frame reported in this report, and further decrease in n_{eff} was observed for the annealed device, however we chose to omit these data points because we observed significant discontinuities in the aging behavior of all three device arrays after a prolonged spike in the storage temperature of the samples. In general, the standard deviation in the calculated $\Gamma_{norm} = 1.0$ intercept for all studies tended to increase over time. For example, calculated error in the Δn_{ChG} of the annealed device for early timepoints was as low as 2.5×10^{-6}, while towards the end of the study the error ranged from 3 to 8×10^{-5}.

Optical Materials EXPRESS

4. Summary

In summary, the change in GSS index over time of the photo-saturated and untreated devices reported in this letter showed good agreement with the Phillips-free axiomatic diffusion to traps model of relaxation, with β values indicating structural relaxation proceeding in response to short range forces within the glass. Photo-saturation of GSS may occur by a somewhat different mechanism, as its β-value is closer to 0.49. The thermally annealed glass exhibits the smallest index drift in the order of 10^{-4}, suggesting that proper heat treatment is the preferred method to stabilize the optical response of ChG devices. The study shows that resonant cavity refractometry can be used as a precise method to extract the aging kinetics of ChG over a relatively short time frame. In addition to shedding light on the aging mechanism, the results also establish the baseline aging behavior of glass undergoing different processing conditions critical for practical photonic device applications based on these materials.

Funding

National Science Foundation (NSF) (1506605).

References

1. R. C. Welch, J. R. Smith, M. Potuzak, X. Guo, B. F. Bowden, T. Kiczenski, D. C. Allan, E. A. King, A. J. Ellison, and J. C. Mauro, "Dynamics of glass relaxation at room temperature," Phys. Rev. Lett. **110**(26), 265901 (2013).
2. S. V. Nemilov, "Physical Ageing of Silicate Glasses at Room Temperature: General Regularities as a Basis for the Theory and the Possibility of a priori Calculation of the Ageing Rate," Glass Phys. Chem. **26**(6), 511–530 (2000).
3. R. D. Priestley, "Physical aging of confined glasses," Soft Matter **5**(5), 919–926 (2009).
4. S. V. Nemilov, "Structural relaxation in oxide glasses at room temperature," Physics and Chemistry of Glasses-European Journal of Glass Science and Technology Part B **48**, 291–295 (2007).
5. J. P. Joule, "The Scientific Papers of Joule J.P.," London Physical Society **1**, 558 (1884).
6. J. Phillips, "Microscopic theory of the Kohlrausch relaxation constant β_K," J. Non-Cryst. Solids **172-174**, 98–103 (1994).
7. J. Phillips, "Stretched exponential relaxation in molecular and electronic glasses," Rep. Prog. Phys. **59**(9), 1133–1207 (1996).
8. J. C. Phillips, "Microscopic aspects of Stretched Exponential Relaxation (SER) in homogeneous molecular and network glasses and polymers," J. Non-Cryst. Solids **357**(22-23), 3853–3865 (2011).
9. J. R. Macdonald and J. C. Phillips, "Topological derivation of shape exponents for stretched exponential relaxation," J. Chem. Phys. **122**(7), 074510 (2005).
10. P. Lucas, "Energy landscape and photoinduced structural changes in chalcogenide glasses," J. Phys.: Condens. Matter **18**(24), 5629–5638 (2006).
11. R. Y. Golovchak, S. A. Kozyukhin, A. Kozdras, O. I. Shpotyuk, and V. M. Novotortsev, "Physical Aging of Chalcogenide Glasses," Inorg. Mater. **46**(8), 911–913 (2010).
12. J. Saiter, "Physical ageing in chalcogenide glasses," J. Optoelectron. Adv. Mater. **3**, 685–694 (2001).
13. O. Shpotyuk, A. Kozdras, V. Balitska, and R. Golovchak, "On the compositional diversity of physical aging kinetics in chalcogenide glasses," J. Non-Cryst. Solids **437**, 1–5 (2016).
14. A. Kozdras, "Kinetics of light-assisted physical ageing in S-rich arsenic sulphide glasses," Bull. Mater. Sci. **39**(4), 997–1000 (2016).
15. R. Golovchak, A. Kozdras, and O. Shpotyuk, "Optical signature of structural relaxation in glassy $As_{10}Se_{90}$," J. Non-Cryst. Solids **356**(23-24), 1149–1152 (2010).
16. D.-Y. Choi, S. Madden, D. Bulla, R. Wang, A. Rode, and B. J. J. o. A. P. Luther-Davies, "Thermal annealing of arsenic tri-sulphide thin film and its influence on device performance," J. Appl. Phys. **107**, 053106 (2010).
17. P. Knotek, P. Kutálek, M. Vlasová, E. Černošková, P. Janíček, Z. Černošek, L. Tichý, and Physics, "Ageing of $Ge_{24.9}Sb_{11.6}S_{63.5}$ thin films under various conditions," Mater. Chem. Phys. **195**, 236–246 (2017).
18. O. Mouawad, P. Vitry, C. Strutynski, J. Picot-Clémente, F. Désévédavy, G. Gadret, J. C. Jules, E. Lesniewska, and F. Smektala, "Atmospheric aging and surface degradation in As_2S_3 fibers in relation with suspended-core profile," Opt. Mater. **44**, 25–32 (2015).
19. R. K. Puri, K. Vijaya, and R. N. Karekar, "Effect of minute's-scale aging on refractive index of chopped and non-chopped optical films," Pramana **21**(5), 311–322 (1983).
20. Y. Zou, H. Lin, O. Ogbuu, L. Li, S. Danto, S. Novak, J. Novak, J. D. Musgraves, K. Richardson, and J. Hu, "Effect of annealing conditions on the physio-chemical properties of spin-coated As_2Se_3 chalcogenide glass films," Opt. Mater. Express **2**(12), 1723–1732 (2012).
21. E. Koontz, V. Blouin, P. Wachtel, J. D. Musgraves, and K. Richardson, "Prony series spectra of structural relaxation in N-BK7 for finite element modeling," J. Phys. Chem. A **116**(50), 12198–12205 (2012).

Optical Materials EXPRESS

22. E. Koontz, "Characterization of structural relaxation in inorganic glasses using length dilatometry," (Clemson University, 2015).
23. J. Lapointe, Y. Ledemi, S. Loranger, V. L. Iezzi, E. Soares de Lima Filho, F. Parent, S. Morency, Y. Messaddeq, and R. Kashyap, "Fabrication of ultrafast laser written low-loss waveguides in flexible As_2S_3 chalcogenide glass tape," Opt. Lett. **41**(2), 203–206 (2016).
24. C. C. Huang, D. W. Hewak, and J. V. Badding, "Deposition and characterization of germanium sulphide glass planar waveguides," Opt. Express **12**(11), 2501–2506 (2004).
25. A. Stone, H. Jain, V. Dierolf, M. Sakakura, Y. Shimotsuma, K. Miura, K. Hirao, J. Lapointe, and R. Kashyap, "Direct laser-writing of ferroelectric single-crystal waveguide architectures in glass for 3D integrated optics," Sci. Rep. **5**(1), 10391 (2015).
26. T. Sabapathy, A. Ayiriveetil, A. K. Kar, S. Asokan, and S. J. Beecher, "Direct ultrafast laser written C-band waveguide amplifier in Er-doped chalcogenide glass," Opt. Mater. Express **2**(11), 1556–1561 (2012).
27. J. Hu, V. Tarasov, N. Carlie, L. Petit, A. Agarwal, K. Richardson, and L. Kimerling, "Exploration of waveguide fabrication from thermally evaporated Ge–Sb–S glass films," Opt. Mater. **30**(10), 1560–1566 (2008).
28. V. Mittal, A. Aghajani, L. G. Carpenter, J. C. Gates, J. Butement, P. G. R. Smith, J. S. Wilkinson, and G. S. Murugan, "Fabrication and characterization of high-contrast mid-infrared $GeTe_4$ channel waveguides," Opt. Lett. **40**(9), 2016–2019 (2015).
29. J. M. Morris, M. D. Mackenzie, C. R. Petersen, G. Demetriou, A. K. Kar, O. Bang, and H. T. Bookey, "$Ge_{22}As_{20}Se_{58}$ glass ultrafast laser inscribed waveguides for mid-IR integrated optics," Opt. Mater. Express **8**(4), 1001–1011 (2018).
30. A. Gutierrez-Arroyo, E. Baudet, L. Bodiou, J. Lemaitre, I. Hardy, F. Faijan, B. Bureau, V. Nazabal, and J. Charrier, "Optical characterization at 7.7 μm of an integrated platform based on chalcogenide waveguides for sensing applications in the mid-infrared," Opt. Express **24**(20), 23109–23117 (2016).
31. X. Gai, T. Han, A. Prasad, S. Madden, D.-Y. Choi, R. Wang, D. Bulla, and B. Luther-Davies, "Progress in optical waveguides fabricated from chalcogenide glasses," Opt. Express **18**(25), 26635–26646 (2010).
32. C. Vigreux, M. V. Thi, G. Maulion, R. Kribich, M. Barillot, V. Kirschner, and A. Pradel, "Wide-range transmitting chalcogenide films and development of micro-components for infrared integrated optics applications," Opt. Mater. Express **4**(8), 1617–1631 (2014).
33. M. Shokooh-Saremi, V. G. Ta'eed, N. J. Baker, I. C. M. Littler, D. J. Moss, B. J. Eggleton, Y. Ruan, and B. Luther-Davies, "High-performance Bragg gratings in chalcogenide rib waveguides written with a modified Sagnac interferometer," J. Opt. Soc. Am. B **23**(7), 1323–1331 (2006).
34. A. Saliminia, A. Villeneuve, T. V. Galstyan, S. LaRochelle, and K. Richardson, "First- and Second-Order Bragg Gratings in Single-Mode Planar Waveguides of Chalcogenide Glasses," J. Lightwave Technol. **17**(5), 837–842 (1999).
35. J. Hu, N. Carlie, L. Petit, A. Agarwal, K. Richardson, and L. Kimerling, "Demonstration of chalcogenide glass racetrack microresonators," Opt. Lett. **33**(8), 761–763 (2008).
36. Y. H. Q. Du, J. Li, D. Kita, J. Michon, H. Lin, L. Li, S. Novak, K. Richardson, W. Zhang, and J. Hu, "Low-loss photonic device in Ge-Sb-S chalcogenide glass," Opt. Lett. **41**(13), 3090–3093 (2016).
37. H. Lin, L. Li, Y. Zou, S. Danto, J. D. Musgraves, K. Richardson, S. Kozacik, M. Murakowski, D. Prather, P. T. Lin, V. Singh, A. Agarwal, L. C. Kimerling, and J. Hu, "Demonstration of high-Q mid-infrared chalcogenide glass-on-silicon resonators," Opt. Lett. **38**(9), 1470–1472 (2013).
38. P. Ma, D.-Y. Choi, Y. Yu, Z. Yang, K. Vu, T. Nguyen, A. Mitchell, B. Luther-Davies, and S. Madden, "High Q factor chalcogenide ring resonators for cavity-enhanced MIR spectroscopic sensing," Opt. Express **23**(15), 19969–19979 (2015).
39. S. Levy, M. Klebanov, and A. Zadok, "High-Q ring resonators directly written in As_2S_3 chalcogenide glass films," Photonics Res. **3**(3), 63–67 (2015).
40. J. H. Choi, D.-H. Cha, J.-H. Kim, and H.-J. Kim, "Development of thermally stable and moldable chalcogenide glass for flexible infrared lenses," J. Mater. Res. **31**(12), 1674–1680 (2016).
41. E. A. Sanchez, M. Waldmann, and C. B. Arnold, "Chalcogenide glass microlenses by inkjet printing," Appl. Opt. **50**(14), 1974–1978 (2011).
42. W. Zhou, L. Zhang, and A. Y. Yi, "Design and fabrication of a compound-eye system using precision molded chalcogenide glass freeform microlens arrays," Optik **171**, 294–303 (2018).
43. P. Sachan, R. Singh, P. K. Dwivedi, and A. Sharma, "Infrared microlenses and gratings of chalcogenide: confined self-organization in solution processed thin liquid films," RSC Adv. **8**(49), 27946–27955 (2018).
44. T. Zhou, Z. Zhu, X. Liu, Z. Liang, and X. Wang, "A Review of the Precision Glass Molding of Chalcogenide Glass (ChG) for Infrared Optics," Micromachines **9**(7), 337 (2018).
45. R. G. DeCorby, N. Ponnampalam, H. T. Nguyen, and T. J. Clement, "Robust and Flexible Free-Standing All-Dielectric Omnidirectional Reflectors," Adv. Mater. **19**(2), 193–196 (2007).
46. H. E. Kondakci, M. Yaman, O. Koylu, A. Dana, and M. Bayindir, "All-chalcogenide glass omnidirectional photonic band gap variable infrared filters," Appl. Phys. Lett. **94**(11), 111110 (2009).
47. J. Wang, T. Zens, J. Hu, P. Becla, L. C. Kimerling, and A. M. Agarwal, "Monolithically integrated, resonant-cavity-enhanced dual-band mid-infrared photodetector on silicon," Appl. Phys. Lett. **100**(21), 211106 (2012).
48. T. Kohoutek, J. Orava, T. Sawada, and H. Fudouzi, "Inverse opal photonic crystal of chalcogenide glass by solution processing," J. Colloid Interface Sci. **353**(2), 454–458 (2011).

Optical Materials EXPRESS

49. D. Freeman, S. Madden, and B. Luther-Davies, "Fabrication of planar photonic crystals in a chalcogenide glass using a focused ion beam," Opt. Express **13**(8), 3079–3086 (2005).
50. H. Lin, L. Li, F. Deng, C. Ni, S. Danto, J. D. Musgraves, K. Richardson, and J. Hu, "Demonstration of mid-infrared waveguide photonic crystal cavities," Opt. Lett. **38**(15), 2779–2782 (2013).
51. P. Zhang, Z. Zhao, J. Zeng, Q. Zhang, X. Wang, F. Chen, X. Shen, and S. Dai, "Fabrication and characterization of $Ge_{20}As_{20}Se_{15}Te_{45}$ chalcogenide glass for photonic crystal by nanoimprint lithography," Opt. Mater. Express **6**(6), 1853–1860 (2016).
52. M. Asobe, "Nonlinear Optical Properties of Chalcogenide Glass Fibers and Their Application to All-Optical Switching," Opt. Fiber Technol. **3**(2), 142–148 (1997).
53. V. G. Ta'eed, N. J. Baker, L. Fu, K. Finsterbusch, M. R. E. Lamont, D. J. Moss, H. C. Nguyen, B. J. Eggleton, D. Y. Choi, S. Madden, and B. Luther-Davies, "Ultrafast all-optical chalcogenide glass photonic circuits," Opt. Express **15**(15), 9205–9221 (2007).
54. J-É. Tremblay, M. Malinowski, K. A. Richardson, S. Fathpour, and M. C. Wu, "Picojoule-level octave-spanning supercontinuum generation in chalcogenide waveguides," Opt. Express **26**(16), 21358–21363 (2018).
55. Q. Du, Z. Luo, H. Zhong, Y. Zhang, Y. Huang, T. Du, W. Zhang, T. Gu, and J. Hu, "Chip-scale broadband spectroscopic chemical sensing using an integrated supercontinuum source in a chalcogenide glass waveguide," Photonics Res. **6**(6), 506–510 (2018).
56. C. R. Petersen, N. Prtljaga, M. Farries, J. Ward, B. Napier, G. R. Lloyd, J. Nallala, N. Stone, and O. Bang, "Mid-infrared multispectral tissue imaging using a chalcogenide fiber supercontinuum source," Opt. Lett. **43**(5), 999–1002 (2018).
57. Y. Yu, X. Gai, T. Wang, P. Ma, R. Wang, Z. Yang, D.-Y. Choi, S. Madden, and B. Luther-Davies, "Mid-infrared supercontinuum generation in chalcogenides," Opt. Mater. Express **3**(8), 1075–1086 (2013).
58. F. Chen and J. R. V. Aldana, "Optical waveguides in crystalline dielectric materials produced by femtosecond-laser micromachining," Laser Photonics Rev. **8**(2), 251–275 (2014).
59. M. R. Vázquez, B. Sotillo, S. Rampini, V. Bharadwaj, B. Gholipour, P. Fernández, R. Ramponi, C. Soci, and S. M. Eaton, "Femtosecond laser inscription of nonlinear photonic circuits in Gallium Lanthanum Sulphide glass," J. Phys. Photonics **1**(1), 015006 (2018).
60. A. Arriola, S. Gross, M. Ams, T. Gretzinger, D. Le Coq, R. P. Wang, H. Ebendorff-Heidepriem, J. Sanghera, S. Bayya, L. B. Shaw, M. Ireland, P. Tuthill, and M. J. Withford, "Mid-infrared astrophotonics: study of ultrafast laser induced index change in compatible materials," Opt. Mater. Express **7**(3), 698–711 (2017).
61. J. Hu, L. Li, H. Lin, P. Zhang, W. Zhou, and Z. Ma, "Flexible integrated photonics: where materials, mechanics and optics meet [Invited]," Opt. Mater. Express **3**(9), 1313–1331 (2013).
62. L. Li, Y. Zou, H. Lin, J. Hu, X. Sun, N. Feng, S. Danto, K. Richardson, T. Gu, and M. Haney, "A Fully-Integrated Flexible Photonic Platform for Chip-to-Chip Optical Interconnects," J. Lightwave Technol. **31**(24), 4080–4086 (2013).
63. L. Li, H. Lin, Y. Huang, R.-J. Shiue, A. Yadav, J. Li, J. Michon, D. Englund, K. Richardson, T. Gu, and J. Hu, "High-performance flexible waveguide-integrated photodetectors," Optica **5**(1), 44–51 (2018).
64. L. Li, H. Lin, S. Qiao, Y. Zou, S. Danto, K. Richardson, J. D. Musgraves, N. Lu, and J. Hu, "Integrated flexible chalcogenide glass photonic devices," Nat. Photonics **8**(8), 643–649 (2014).
65. L. Li, H. Lin, S. Qiao, Y.-Z. Huang, J.-Y. Li, J. Michon, T. Gu, C. Alosno-Ramos, L. Vivien, and A. Yadav, "Monolithically integrated stretchable photonics," Light: Sci. Appl. **7**(2), 17138 (2018).
66. L. Li, H. Lin, J. Michon, Y. Huang, J. Li, Q. Du, A. Yadav, K. Richardson, T. Gu, and J. Hu, "A new twist on glass: A brittle material enabling flexible integrated photonics," Int. J. Appl. Glass Sci. **8**(1), 61–68 (2017).
67. Y. Zou, L. Moreel, H. Lin, J. Zhou, L. Li, S. Danto, J. D. Musgraves, E. Koontz, K. Richardson, K. D. Dobson, R. Birkmire, and J. Hu, "Solution Processing and Resist-Free Nanoimprint Fabrication of Thin Film Chalcogenide Glass Devices: Inorganic–Organic Hybrid Photonic Integration," Adv. Opt. Mater. **2**(8), 759–764 (2014).
68. J. Choi, N. Carlie, L. Petit, T. Anderson, K. Richardson, and M. Richardson, "Measurement of Photo-Induced Refractive Index Change in $As_{0.42-x-y}Ge_xSb_yS_{0.58}$ Bulks Induced by Fs Near IR Laser Exposure," in *LEOS 2007 - IEEE Lasers and Electro-Optics Society Annual Meeting Conference Proceedings*, 2007), 100–101.
69. I. Camlibel, D. Pinnow, and F. Dabby, "Optical aging characteristics of borosilicate clad fused silica core fiber optical waveguides," Appl. Phys. Lett. **26**(4), 185–187 (1975).
70. B. Bureau, X. H. Zhang, F. Smektala, J.-L. Adam, J. Troles, H.-l. Ma, C. Boussard-Plèdel, J. Lucas, P. Lucas, and D. Le Coq, "Recent advances in chalcogenide glasses," J. Non-Cryst. Solids **345–346**, 276–283 (2004).
71. M. Churbanov, V. Shiryaev, V. Gerasimenko, A. Pushkin, I. Skripachev, G. Snopatin, and V. Plotnichenko, "Stability of the optical and mechanical properties of chalcogenide fibers," Inorg. Mater. **38**(10), 1063–1068 (2002).
72. K. Richardson, C. Lopez, A. Schulte, C. Rivero, A. Saliminia, T. Galstian, K. Turcotte, A. Villeneuve, T. Cardinal, and M. Couzi, "Aging Behavior of Photo-Induced As_2S_3 Gratings," in *Conference on Lasers and Electro-Optics*, (Optical Society of America, 2001), CTuM29.
73. V. Lubchenko and P. G. Wolynes, "Theory of aging in structural glasses," J. Chem. Phys. **121**(7), 2852–2865 (2004).
74. J. C. Dyre, "Heirs of liquid treasures," Nat. Mater. **3**(11), 749–750 (2004).
75. J. C. Dyre, "Source of non-Arrhenius average relaxation time in glass-forming liquids," J. Non-Cryst. Solids **235-237**, 142–149 (1998).

Optical Materials EXPRESS

76. J. M. Saiter, M. Arnoult, and J. Grenet, "Very long physical ageing in inorganic polymers exemplified by the GexSe1−x vitreous system," Phys. B **355**(1-4), 370–376 (2005).
77. R. Golovchak, A. Kovalskiy, O. Shpotyuk, and H. Jain, "In search of energy landscape for network glasses," Appl. Phys. Lett. **98**(17), 171905 (2011).
78. R. Golovchak, A. Kozdras, O. Shpotyuk, and V. Balitska, "Crossover between cooperative and fractal relaxation in complex glass-formers," J. Phys.: Condens. Matter **28**(35), 355101 (2016).
79. J. Hu, unpublished results. Data available upon request.
80. J. Hu, N. Carlie, N.-N. Feng, L. Petit, A. Agarwal, K. Richardson, and L. Kimerling, "Planar waveguide-coupled, high-index-contrast, high-Q resonators in chalcogenide glass for sensing," Opt. Lett. **33**(21), 2500–2502 (2008).
81. M. Åslund and J. Canning, "Annealing properties of gratings written into UV-presensitized hydrogen-outdiffused optical fiber," Opt. Lett. **25**(10), 692–694 (2000).
82. L. Li, P. Zhang, W.-M. Wang, H. Lin, A. B. Zerdoum, S. J. Geiger, Y. Liu, N. Xiao, Y. Zou, and O. Ogbuu, "Foldable and cytocompatible sol-gel TiO_2 photonics," Sci. Rep. **5**(1), 13832 (2015).
83. H. Lin, Y. Song, Y. Huang, D. Kita, S. Deckoff-Jones, K. Wang, L. Li, J. Li, H. Zheng, and Z. Luo, "Chalcogenide glass-on-graphene photonics," Nat. Photonics **11**(12), 798–805 (2017).
84. J. Hu, L. Li, H. Lin, Y. Zou, Q. Du, C. Smith, S. Novak, K. Richardson, and J. D. Musgraves, "Chalcogenide glass microphotonics: Stepping into the spotlight," Am. Ceram. Soc. Bull. **94**, 24–29 (2015).
85. C. Smith, J. Jackson, L. Petit, C. Rivero-Baleine, and K. Richardson, "Processing and characterization of new oxy-sulfo-telluride glasses in the Ge–Sb–Te–S–O system," J. Solid State Chem. **183**(8), 1891–1899 (2010).
86. C. Ping, P. Boolchand, and D. G. Georgiev, "Long term aging of selenide glasses: evidence of sub-T_g endotherms and pre-T_g exotherms," J. Phys.: Condens. Matter **22**(6), 065104 (2010).
87. J. D. Musgraves, N. Carlie, J. Hu, L. Petit, A. Agarwal, L. C. Kimerling, and K. A. Richardson, "Comparison of the optical, thermal and structural properties of Ge–Sb–S thin films deposited using thermal evaporation and pulsed laser deposition techniques," Acta Mater. **59**(12), 5032–5039 (2011).
88. L. Zhang, J. Ding, H. Zheng, S. An, H. Lin, B. Zheng, Q. Du, G. Yin, J. Michon, and Y. Zhang, "Ultra-thin high-efficiency mid-infrared transmissive Huygens meta-optics," Nat. Commun. **9**(1), 1481 (2018).
89. Q. Du, Y. Huang, J. Li, D. Kita, J. Michon, H. Lin, L. Li, S. Novak, K. Richardson, and W. Zhang, "Low-loss photonic device in Ge–Sb–S chalcogenide glass," Opt. Lett. **41**(13), 3090–3093 (2016).
90. J. T. Robinson, K. Preston, O. Painter, and M. Lipson, "First-principle derivation of gain in high-index-contrast waveguides," Opt. Express **16**(21), 16659–16669 (2008).
91. G. Yang, H. Jain, A. Ganjoo, D. Zhao, Y. Xu, H. Zeng, and G. Chen, "A photo-stable chalcogenide glass," Opt. Express **16**(14), 10565–10571 (2008).
92. H. Y. Tang, W. H. Wong, and E. Y. B. Pun, "Long period polymer waveguide grating device with positive temperature sensitivity," Appl. Phys. B: Lasers Opt. **79**(1), 95–98 (2004).
93. P. Knotek, L. Tichy, and P. Kutalek, "Photo-induced effects of the virgin $Ge_{24.9}Sb_{11.6}S_{63.5}$ film," Thin Solid Films **594**, 67–73 (2015).